*Inorg. Chem.* **2003**, *42*, 335–347


# Compositional and $^2$H NMR Studies of Bis(benzene)chromium Composites of Mesoporous Vanadium–Niobium Mixed Oxides

**Xun He,[†] Andy Y. H. Lo,[†] Michel Trudeau,[‡] Robert W. Schurko,[†] and David Antonelli*[,†]**

*Department of Chemistry and Biochemistry, University of Windsor, 401 Sunset Avenue, Windsor, Ontario N9B-3P4, Canada, and Emerging Technologies, Hydro-Québec Research Institute, 1800 Boulevard Lionel-Boulet, Varennes, Quebec J3X 1S1, Canada*

Received September 13, 2002

New mesoporous niobium oxides with 5, 10, and 15 mol % vanadium(V) doped into the walls of the structure were synthesized by the ligand-assisted templating method with an octadecylamine template. These materials were characterized by XRD, XPS, EPR, elemental analysis, and nitrogen adsorption before being treated with excess bis(benzene)chromium to give new composites with an organometallic phase in the walls. All materials were also characterized by EPR, XRD, nitrogen adsorption, XPS, SQUID magnetometry, and elemental analysis. The materials with higher percentages of vanadium absorbed more bis(benzene)chromium, because this process depends largely on the electron transfer between the organometallic and the walls of the mesostructure and vanadium(V) is a stronger oxidant than niobium(V). Conductivity studies on these materials revealed that the ratio of Cr(0) to Cr(I) in the pores was more important than the absolute Cr loading level in governing electron transport properties but that increasing the V content led to more insulating behavior regardless of the Cr concentration. Solid-state $^2$H NMR studies on perdeuteriobenzene analogues of these composites showed the presence of the neutral and cationic Cr species in different ratios depending on the loading. Tumbling of these species was also slow on the NMR time scale, indicating that the charge-carrying Cr species are not rapidly moving through the pore channels of the mesostructure. This suggests that the walls of the structure may play a key role in charge transfer in these composites, contrary to what was previously believed.

## Introduction

The study of the synthesis and physical properties of nanoporous materials is one of the fastest growing areas in materials science. By exploiting structure property relations in nanostructured inorganic composites, it is possible to fabricate materials in which the local composition, grain size, and porosity can be tuned to give the desired macroscopic properties. Mesoporous materials[1−6] are important as hosts for organic and inorganic guest phases because the 20−500 Å pore sizes allow encapsulation of species too large to be introduced into the pore cavities of zeolites.[7] The extension of this class of materials from main group oxides to transition metals is of particular importance because transition metals possess variable oxidation states which are important in magnetic, optical, and electronic properties of many materials.[8−13] Recently we showed that mesoporous Nb, Ta, and Ti oxides can act as potent electron acceptors in host−

* Author to whom correspondence should be addressed. E-mail: danton@uwindsor.ca.
[†] University of Windsor.
[‡] Hydro-Québec Research Institute.

(1) (a) Kresge, C. T.; Leonowicz, M. E.; Roth, W. J.; Vartulli, J. C.; Beck, J. S. *Nature* **1992**, *359*, 710. (b) Beck, J. S.; Vartuli, J. C.; Roth, W. J.; Leonowicz, M. E.; Kresge, C. T.; Schmitt, K. D.; Chu, C. T.-W.; Olson, D. H.; Shepard, E. W.; McCullen, S. B.; Higgins, J. B.; Schlenker, J. L. *J. Am. Chem. Soc.* **1992**, *114*, 10834.
(2) (a) Huo, Q.; Margolese, D. I.; Ciesla, U.; Demuth, D. G.; Feng, P.; Gier, T. E.; Sieger, P.; Firouzi, A.; Chmelka, B. F.; Schuth, F.; Stucky, G. D. *Chem. Mater.* **1994**, *6*, 1176; (b) Firouzi, A.; Kumar, D.; Bull, L. M.; Besier, T.; Sieger, P.; Huo, Q., Walker, S. A.; Zasadzinski, J. A.; Glinka, C.; Nicol, J.; Margolese, D.; Stucky, G. D.; Chmelka, B. F. *Science* **1995**, *267*, 1138.
(3) Chen, C.-Y.; Burkette, S. L.; Li, H.-X.; Davis, M. E. *Microporous Mater.* **1993**, *2*, 27.
(4) Tanev, P. T.; Chibwe, M.; Pinnavaia, T. J. *Nature* **1994**, *368*, 321.
(5) (a) Antonelli, D. M.; Ying, J. Y. *Curr. Opin. Colloid Interface Sci.* **1996**, *1*, 523.
(6) Behrens, P. *Angew. Chem., Int. Ed. Engl.* **1996**, *35*, 515.
(7) (a) Wu, C. G.; Bein, T. *Science* **1994**, *264*, 1757. (b) Wu, C.-G.; Bein, T. *Chem. Mater.* **1994**, *6*, 1109.
(8) (a) Antonelli, D. M.; Ying, J. Y. *Angew. Chem., Int. Ed. Engl.* **1996**, *35*, 426. (b) Antonelli, D. M.; Nakahira, A.; Ying, J. Y. *Inorg. Chem.* **1996**, *35*, 3126. (c) Antonelli, D. M.; Ying, J. Y. *Angew. Chem., Int. Ed. Engl.* **1995**, *34*, 2014. (d) Antonelli, D. M.; Ying, J. Y. *Chem. Mater.* **1996**, *8*, 874.
(9) Tian, Z. R.; Wang, J. Y.; Duan, N. G.; Krishnan, V. V.; Suib, S. L. *Science* **1997**, *276*, 926.
(10) Mamak, M.; Coombs, N.; Ozin, G. *Adv. Mater.* **2000**, *12*, 198.
(11) Liu, P.; Liu, J.; Sayari, A. *Chem. Commun.* **1997**, 577.

10.1021/ic020559v CCC: $25.00 
Published on Web 12/18/2002

guest inclusion reactions involving alkali metals,[14−16] alkali metal fullerides,[17] and a wide range of bis(arene) and bis(cyclopentadienyl) complexes.[18−23] The controlled porosity and electrochemical activity of these mesoporous oxides allow us to couple quantum confinement and the introduction of hole defects into the guest species in a single step. The reaction of mesoporous niobium oxide with bis(benzene)chromium leads to semiconducting materials with a mixed oxidation state organometallic phase in the pores.[21] However, only small amounts (<1 wt %) of bis(benzene)chromium are oxidized by the mesoporous niobium oxide due to the limited availability of low-lying acceptor states in the niobium oxide phase strong enough to oxidize the organometallic. To conduct a study of the variation of electronic properties with the bis(benzene)chromium loading level, it is therefore necessary to increase the oxidizing ability of the mesostructure by doping it with a more highly oxidizing species. Herein, we report the synthesis of a new family of V-doped mesoporous niobium oxide materials in which the V content in the walls controls the level of bis(benzene)chromium in the structure by tuning the ability of the structure to function as an oxidizing agent. Solid-state $^2$H NMR experiments were also conducted on the perdeutero analogues of these composites to probe into the dynamic behavior of the Cr species in the pores.

## Experimental Section

**Materials and Equipment.** All chemicals unless otherwise stated were obtained from Aldrich. Bis(benzene)chromium was obtained from Strem Chemicals. Trimethylsilyl chloride was distilled over calcium hydride. Bis(hexadeuteriobenzene)chromium was synthesized according to the literature,[24] but perdeuteriobenzene was in place of benzene as starting reagent. Bis(benzene)chromium iodide and bis(hexadeuteriobenzene)chromium iodide were made according to the literature.[25] Mesoporous niobium oxide was made according to the method of Antonelli and Ying.[8]

Nitrogen adsorption and desorption data were collected on a Micromeritics ASAP 2010. X-ray diffraction (XRD) patterns (Cu K$\alpha$) were recorded in a sealed glass capillary on a Siemens D-500 $\theta-2\theta$ diffractometer. All X-ray photoelectron spectroscopy (XPS) emissions were referenced to the carbon C−(C, H) peak at 284.8 eV, and the data were obtained using a Physical Electronics PHI-5500 using charge neutralization. The conductivity measurements were recorded on a Jandel 4-point universal probe head combined with a Jandel resistivity unit. The equations used for calculating the resistivity were as follows.

For pellets of <0.5 mm thickness,

$$\rho = \left(\frac{\pi}{\log n^2}\frac{V}{I}\right)t$$

For pellets of >0.5 mm thickness, the following equation is used:

$$\rho = 2\pi(S)\frac{V}{I}$$

Here $\rho$ = resistivity, $\pi/\log n^2$ = sheet resistivity, $V$ = volts, $I$ = current, $t$ = thickness of the pellet, and $S$ = the spacing of the probes (0.1 cm). For variable-temperature resistivity measurements pressed pellets with four copper wires affixed by conducting silver adhesive (Alfa Aesar) were coated in epoxy resin in a glovebox. Samples were cooled from room temperature to liquid-nitrogen temperature while transport measurements were made using a Keithly programmable current source and voltmeter.

The powder electron paramagnetic resonance (EPR) samples were prepared under vacuum and the data collected on a Brüker X-band ESP 300E EPR spectrometer. Magnetic measurements were conducted on a Quantum Design SQUID magnetometer MPMS system with a 5 T magnet. Solid-state variable-temperature (VT) $^2$H NMR experiments were conducted on a Varian Infinity Plus 9.4 T wide-bore NMR spectrometer at $\upsilon_0 = 61.4$ MHz using Varian/Chemagnetics 5 mm wide-line and 5 mm HXY MAS (in single-resonance $^2$H mode) probes. For both stationary and spinning samples, a quadrupolar echo pulse sequence of the form $(\pi/2)_x-\tau-(\pi/2)_y-\tau-$acquire was applied.[26] A single set of rotor-synchronized quadrupolar echo magic-angle spinning (MAS) NMR experiments with spinning frequencies $\nu_{rot}$ of 9.1 and 11.0 kHz were conducted on the mesoporous niobium oxide loaded with 0.1 equiv of bis(benzene)chromium(0). Sample temperatures were varied from −150 to +100 °C. Samples were carefully powdered and packed into 5 mm o.d. Teflon tubes or 5 mm o.d. zirconium oxide rotors and sealed with airtight caps. All $^2$H NMR spectra were referenced with respect to TMS, $\delta = 0.0$ ppm, by using benzene-$d_6$ as a secondary reference with $\delta = 7.27$ ppm. The 90° pulses ranged from 2.5 to 3.1 $\mu$s for experiments with the 5 mm wide-line probe and 4.6 $\mu$s for MAS experiments, corresponding to rf fields ranging from $\upsilon_1 = 54.3$ to 80.7 kHz. The interpulse delays in the quadrupolar echo sequence, $\tau$, were 200 or 520 $\mu$s in the static experiments and $1/\nu_{rot}$ in the MAS experiments. The static NMR experiments on pure samples of bis(benzene)chromium(0) and the bis(benzene)chromium(I) cation required the acquisition of ca. 200 to 2000 transients with pulse delays of 1 and 0.5 s, respectively. Static experiments on the loaded mesoporous niobium oxides required acquisition of ca. 4000 transients with a pulse delay of 0.5 s, while the MAS experiments required 368 scans. Solid-state $^1$H MAS NMR experiments were conducted on the bis(benzene)chromium cation at $\upsilon_0 = 400.1$ MHz, using a Varian/Chemagnetics 2.5 mm HX MAS probe, with a spinning frequency of 25 kHz. This sample was packed into a 2.5 mm o.d. zirconium oxide rotor and was referenced with respect to dichloromethane ($\delta = 5.3$ ppm). The 90° pulse width was 2.7 $\mu$s, and $\upsilon_1 = 92.6$ kHz. The acquisition required 16 scans with 4 s recycle delay. The quadrupolar coupling

(12) Ciesla, U.; Demuth, D.; Leon, R.; Petroff, P.; Stucky, G.; Unger, K.; Schuth, F. J. *Chem. Soc., Chem. Commun.* **1994**, 1387.
(13) Antonelli, D. M.; Trudeau, M. *Angew. Chem., Int. Ed. Engl.* **1999**, *38*, 1471.
(14) He, X.; Antonelli, D. M. *Angew. Chem., Int. Ed.* **2002**, *41*, 214.
(15) Vettraino, M.; Trudeau, M.; Antonelli, D. M. *Adv. Mater.* **2000**, *12*, 337.
(16) Vettraino, M.; Trudeau, M.; Antonelli, D. M. *Inorg. Chem.* **2001**, *40*, 2088.
(17) (a) Ye, B.; Trudeau, M.; Antonelli, D. M. *Adv. Mater.* **2001**, *13*, 29. (b) Ye, B.; Trudeau, M.; Antonelli, D. M. *Adv. Mater.* **2001**, *13*, 561. (c) Ye, B.; Trudeau, M.; Antonelli, D. M. *Chem. Mater.* **2002**, *14*, 2774.
(18) Murray, S.; Trudeau, M.; Antonelli, D. M. *Adv. Mater.* **2000**, *12*, 1339.
(19) Murray, S.; Trudeau, M.; Antonelli, D. M. *Inorg. Chem.* **2000**, *39*, 5901.
(20) Vettraino, M.; He, X.; Trudeau, M.; Antonelli, D. M. *J. Mater. Chem.* **2001**, *11*, 1.
(21) He, X.; Trudeau, M.; Antonelli, D. M. *Adv. Mater.* **2000**, *12*, 1036.
(22) He, X.; Trudeau, M.; Antonelli, D. M. *Inorg. Chem.* **2001**, *40*, 6463.
(23) He, X.; Trudeau, M.; Antonelli, D. M. *Chem. Mater.* **2001**, *13*, 4808.
(24) Fischer, E. O. *Inorg. Synth.* **1960**, *6*, 132. Fischer, E. O.; Hafner, W. *Z. Anorg. Allg. Chem.* **1956**, *286*, 146.
(25) Fischer, E. O. *Inorg. Synth.* **1960**, *6*, 136.
(26) Chandrakumar, N. *Spin-1 NMR*; Springer-Verlag: New York, 1996.

constants ($C_Q$), the asymmetry parameters ($\eta_Q$), and the isotropic chemical shifts ($\delta_{iso}$) of most of the $^2$H NMR spectra were obtained from spectral simulations using the WSOLIDS software package, which was developed by Dr. Klaus Eichele in Prof. Wasylishen's laboratory at Dalhousie University. WSOLIDS incorporates the space-tiling method of Alderman et al. for the generation of frequency domain solid-state NMR powder patterns.[27] The effect of dynamic motion of the benzene rings on the solid-state $^2$H spectra of bis(benzene)chromium(0) was simulated using the program MXQET[28] on a Dell Precision 420 workstation with dual 733 MHz pentium III processor running Red Hat Linux 6.2. All elemental analysis data (conducted under an inert atmosphere) were obtained from Galbraith Laboratories, 2323 Sycamore Drive, Knoxville, TN 37921-1700.

**Synthesis.** Mesoporous V−Nb mixed oxides were prepared by the ligand-assisted templating method,[8] except 5, 10, or 15 mol % of vanadium(V) triisopropoxy oxide with respect to Nb was added to the Nb(V) ethoxide prior to addition of the octadecylamine template and subsequent hydrolysis/condensation steps. Elemental analysis gave the following results respectively for the three as-synthesized samples (%): **1**, Nb, 45.31; V, 1.30; C, 0.50; H, 2.09; N, less than 0.03; O, 50.70; **2**, Nb, 40.41; V, 1.80; C, 2.01; H, 2.29; N, less than 0.03; O, 53.39; **3**, Nb, 42.80; V, 3.45; C, 0.51; H, 2.40; N, less than 0.03; O, 50.79. The elemental formula of these materials can be calculated as $Nb_{1.0}V_{0.05}O_{6.5}C_{0.09}H_{4.7}$, $Nb_{1.0}V_{0.08}O_{7.7}C_{0.4}H_{5.3}$, and $Nb_{1.0}V_{0.15}O_{6.9}C_{0.09}H_{5.2}$ respectively for **1**−**3**.

Bis(benzene)chromium-reduced mesoporous V−Nb oxide composites (**7**−**9**) were synthesized by addition to a suspension of the trimethylsilyl chloride treated mesoporous V−Nb oxide (**4**, **5**, or **6**) in dry benzene an excess of bis(benzene)chromium calculated on the basis of sample weight and percentage of Nb. The mesoporous solid immediately turns from light yellow to gray-yellow. After several days of additional stirring to ensure complete absorption of the organometallic, the reduced material is collected by suction filtration and washed several times with benzene. Once synthesized, the material is dried in vacuo at $10^{-3}$ Torr on a Schlenk line until all the condensed volatiles had been removed. All reduced oxides in this study were prepared in an analogous fashion. The C and H elemental analysis is summarized in Table 3.

## Results and Discussion

**Characterization of V-Doped Mesoporous Niobium Oxides.** The nitrogen adsorption and desorption isotherms of the mesoporous V−Nb oxides **1**−**3** are shown in Figure 1. The BET surface area, HK pore size, and pore volume of these samples are summarized in Table 1 and compared to a sample of mesoporous niobium oxide prepared without addition of the V dopant. The type IV isotherm exhibited in all cases is indicative of mesoporosity, while the lack of hysteresis demonstrates that the template was removed successfully without significant loss of structure.

Plots of incremental pore volume versus average pore diameter for materials **1**−**3** indicate that these materials possess a narrow pore size distribution (ca. 7 Å width at half-height) upon removal of the template. The powder X-ray diffraction (XRD) patterns show a broad peak centered at $d(100)$ spacing = 40 Å for these materials (Figure 2), consistent with a wormhole pore structure typical of other mesoporous transition metal oxides.

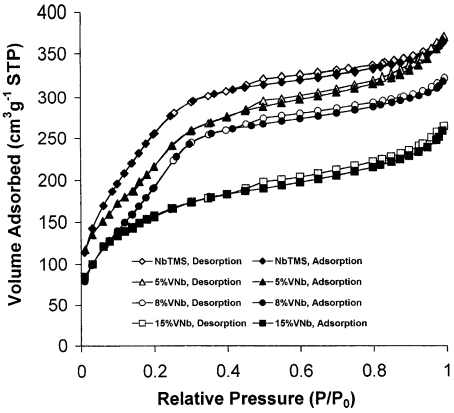


**Figure 1.** Nitrogen adsorption and desorption isotherms of pure mesoporous niobium oxide (Nb−TMS) and vanadium-doped niobium oxide (**1**−**3**).

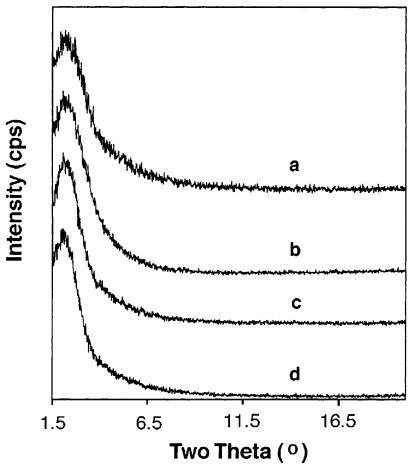


**Figure 2.** XRD patterns of (a) mesoporous niobium oxide, (b) **1**, (c) **2**, and (d) **3**.

**Table 1.** BET Surface Area, Pore Size, and Pore Volume of the As-Synthesized Vanadium-Doped Mesoporous Niobium Oxides

| samples | BET surface area ($m^2$ $g^{-1}$) | HK pore size (Å) | pore vol ($cm^3$ $g^{-1}$) |
|---|---|---|---|
| Nb−TMS | 861 | 23.1 | 0.531 |
| meso-5% VNb (**1**) | 832 | 25.7 | 0.511 |
| meso-8% VNb (**2**) | 761 | 24.0 | 0.436 |
| meso-15% VNb (**3**) | 538 | 23.2 | 0.341 |

Figure 3 shows electron paramagnetic resonance (EPR) spectra of material **1**. The three vanadium-doped samples show similar hyperfine splittings originating from the $^{51}$V nucleus ($I$ = 7/2). These splittings are the combination of double eight lines as vanadium nucleus is parallel (eight lines) and perpendicular (eight lines) to the magnetic field. The simulation of this spectrum gave the hyperfine splitting Hamiltonian parameter $A$ and $g$ values $A(x, x)$ = 76.50 G, $A(y, y)$ = 76.50 G, $A(z, z)$ = 191.50 G, $g(x)$ = 1.979, $g(y)$ = 1.979, and $g(z)$ = 1.929, indicative of vanadium(IV) in the sample.[29] The clear hyperfine splitting indicates that the vanadium(IV) species is well dispersed throughout the Nb oxide bulk structure, otherwise the vanadium nuclei with

(27) Alderman, D. W.; Solum, M. S.; Grant, D. M. *J. Chem. Phys.* **1986**, *84*, 3717−3725.
(28) Greenfield, M. S.; Ronemus, A. D.; Vold, R. L.; Vold, R. R.; Ellis, P. D.; Raidy, T. E. *J. Magn. Reson.* **1987**, *72*, 89−107.

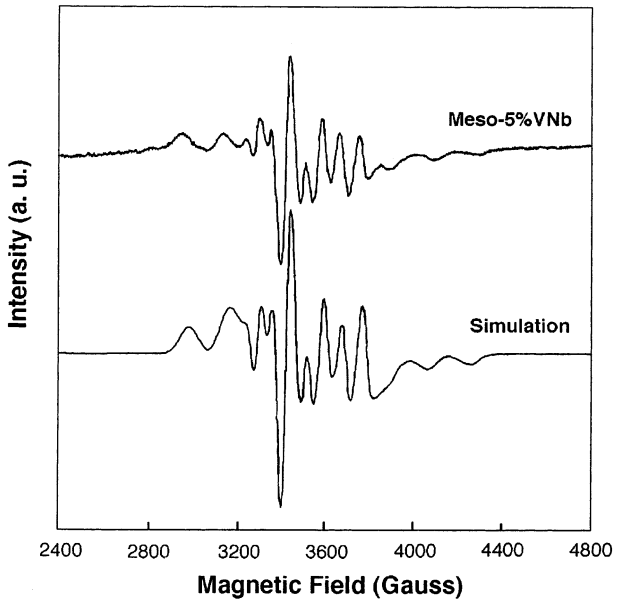


**Figure 3.** Powder EPR spectrum of **1** and the simulation of this spectrum.

unpaired electrons would interact with each other resulting in hyperfine splitting disappearance. The presence of V(IV) in the sample can be accounted for by reduction of the V(V) during the synthesis process, possibly by 2-propanol formed by hydrolysis of the V precursor. Since V(V) is not spin active, it is not possible to determine by this method the ratio between V(IV) and V(V) in the material. When the sample was heated at 100 °C for 4 h, the EPR signal from vanadium(IV) disappeared, indicating that the V species had been completely oxidized into vanadium(V). The nitrogen adsorption and desorption data showed the mesostructure was completely retained after oxidation of V(IV), suggesting that this method is an effective way to produce single-valent vanadium(V)-doped mesoporous niobium oxides.

The X-ray photoelectron (XPS) spectra of **1**−**3** are shown in Figure 4: Figure 4a shows the V 2p 1/2, 3/2 regions with a series of asymmetric emissions which can be assigned to a mixture of V(V) (516.5, 524.1 eV) and V(IV) (515.0, 522.2 eV) according to the literature values for the corresponding oxides.[30] As expected, the intensity of the peaks increases monotonically with the increase in V content. Since XPS is a surface technique, it is difficult to determine the degree of V dispersion through the material; however since the V dopant was introduced as a mixture with the Nb ethoxide precursor and not later in the preparation after a significant degree of condesation of the Nb structure had ensued, it is likely that the V is evenly dispersed throughout and not only on the surface. In related work we have found that elemental percentages of dopants at the surface as determined by XPS are generally reflective of percentages obtained by ICP.[13] Individual crystallites of V oxide are ruled out because of lack of higher angle XRD reflections. Figure 4b shows the Nb 3d region with the 5/2 and 3/2 emissions located at 207.6 and 210.4 eV, consistent with Nb(V).[21] The valence regions near the Fermi level are shown in Figure 4c, yielding an approximate distance to the Fermi level of 3.0 eV for oxygen 2p valence emission. There are no other emissions near the Fermi level which may indicate the presence of metallic states or impurities in the sample. Examination of emissions in this region are important in rationalizing electronic behavior of solid-state materials.

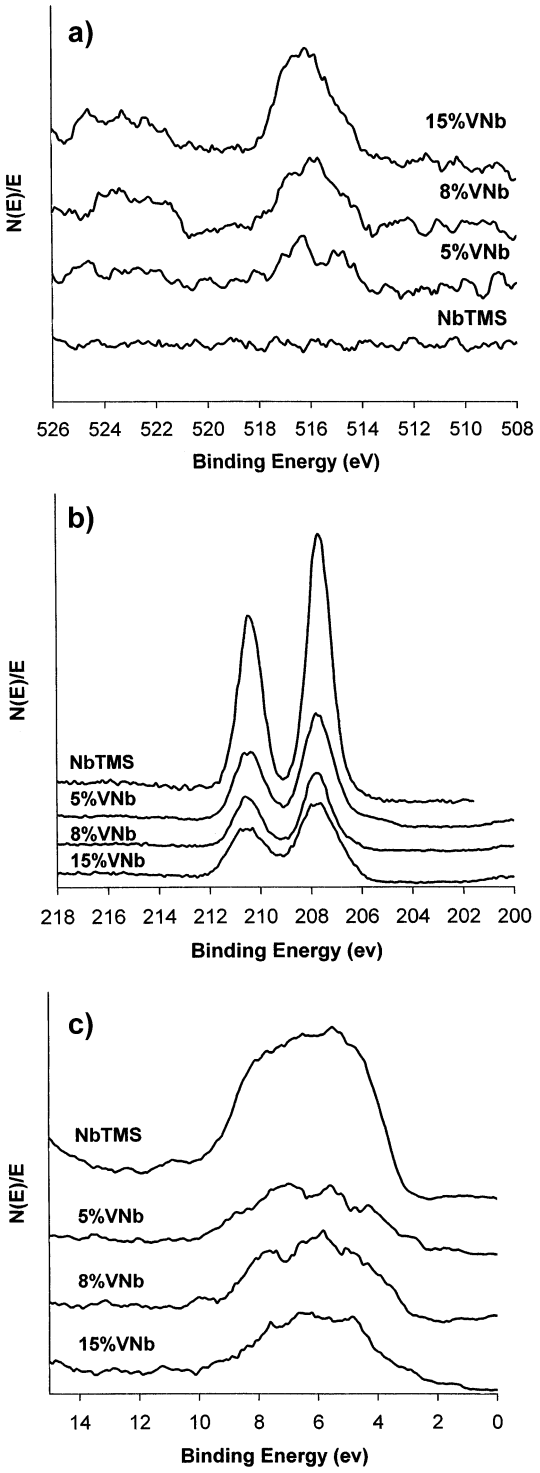


**Figure 4.** XPS spectra of all materials from Figure 1 showing the (a) V 2p 1/2 and 3/2 region, (b) Nb 3d 3/2 and 5/2 region, and (c) region near Fermi level.

(29) Bogomolova, L. D.; Stefanovsky, S. V.; Troole, A. Y.; Vance, E. R. *J. Mater. Sci.* **2001**, *36*, 1213.
(30) (a) Biener, J.; Bäumer, M.; Wang, J.; Madix, R. *Surf. Sci*. **2000**, *450*, 12. (b) Mendialdua, J.; Casanova, R.; Barbaux, Y. *J. Electron Spectrosc. Relat. Phenom*. **1995**, *71*, 249.

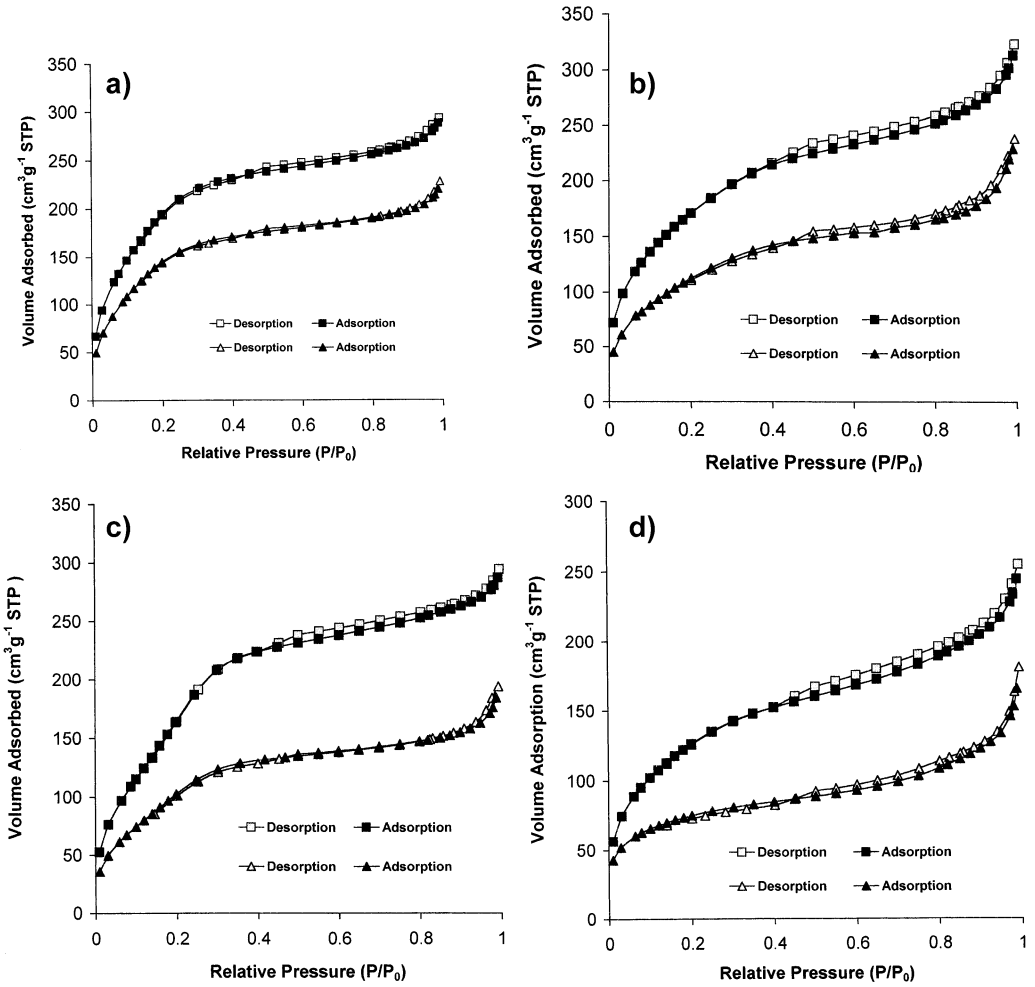


**Figure 5.** Nitrogen adsorption and desorption isotherms of (a) trimethylsilated mesoporous niobium oxide before (top) and after (bottom) treatment with excess bis(benzene)chromium, (b) trimethylsilated **1** (**4**) before (top) and after (**7**) (bottom) treatment with excess bis(benzene)chromium, (c) trimethylsilated **2** (**5**) before (top) and after (**8**) (bottom) treatment with excess bis(benzene)chromium, and (d) trimethylsilated **3** (**6**) before (top) and after (**9**) (bottom) treatment with excess bis(benzene)chromium.

**Synthesis and Characterization of Bis(benzene)chromium Mesoporous V/Nb Oxide Composites.** In a preliminary step, samples of **1**−**3** were treated with excess trimethylsilyl chloride to give materials **4**−**6**. This procedure is necessary to preserving the integrity of the mesostructure after reduction, because it removes water or caps surface hydroxyl groups which form nucleophilic oxygen species, detrimental to the structure, upon reduction. Materials **4**−**6** were then treated with excess bis(benzene)chromium over several days to ensure complete reaction to give reduced composites **7**−**9**. The BET surface area, HK pore size, and pore volume for all reduced samples are shown in Table 2.

The nitrogen adsorption and desorption isotherms of these materials before and after reduction with bis(benzene)-chromium are shown in Figure 5. The loss of surface area exhibited in these isotherms is a consequence of surface coating and pore blockage by the organic and organometallic species and has been commented on previously.[22] The XRD patterns of all new materials exhibited the same *d* spacing as the starting material (Figure 6), indicating retention of the mesostructure on reduction by the organometallic. The elemental analysis of these new materials shows an increase of carbon and hydrogen percentage on intercalation, further confirming that the organometallic was absorbed into the pore structure. The results are summarized in the Table 3. The weight percentage of Cr can be estimated from the increase in carbon on intercalation and the Cr/C weight ratio in the organometallic as 0.97%, 1.27%, and 2.18% for **7**−**9**, respectively. In previous studies on bis(arene) and bis-(cyclopentadienyl) composites of mesoporous Nb oxide, the metal percentage from inductively coupled plasma analysis

**Table 2.** BET Surface Area, Pore Size, and Pore Volume of Trimethylsilylated Vanadium-Doped Mesoporous Niobium Oxides and the Corresponding Bis(benzene) chromium Composites[a]

| samples | BET surf area ($m^2$ $g^{-1}$) | HK pore size (Å) | pore vol ($cm^3$ $g^{-1}$) |
|---|---|---|---|
| Nb−TMS | 771 | 23.1 | 0.434 |
| meso-5% VNb (**4**) | 721 | 25.7 | 0.412 |
| meso-8% VNb (**5**) | 691 | 24.0 | 0.388 |
| meso-15% VNb (**6**) | 457 | 23.2 | 0.331 |
| NbCr | 642 | 22.0 | 0.364 |
| 5% VNbCr (**7**) | 557 | 23.2 | 0.332 |
| 8% VNbCr (**8**) | 487 | 23.0 | 0.286 |
| 15% VNbCr (**9**) | 296 | 22.2 | 0.182 |

[a] The data for pure trimethylsilylated mesoporous niobium oxide synthesized with an octadecylamine template before and after treatment with bis(benzene)chromium are also shown.

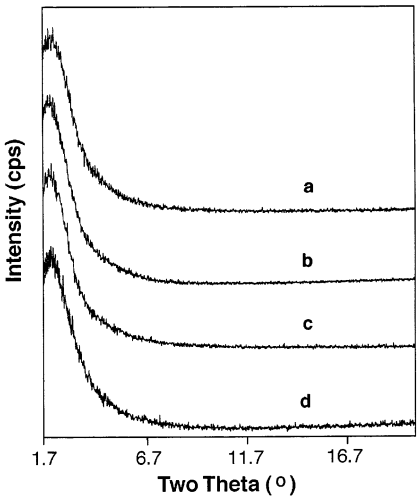


**Figure 6.** XRD patterns of mesoporous transition metal oxides from Figure 1 after treatment with excess bis(benzene)chromium: (a) mesoporous niobium oxide; (b) **7**; (c) **8**; (d) **9**.

**Table 3.** Carbon and Hydrogen Elemental Analysis Results of the Mesoporous Transition Metal Oxides before and after Reduction with Bis(benzene)chromium

| samples before redn | carbon (wt %) | hydrogen (wt %) | samples after redn | carbon (wt %) | hydrogen (wt %) |
|---|---|---|---|---|---|
| Nb−TMS1 | 5.73 | 1.43 | NbCr | 7.24 | 1.75 |
| meso-5% VNb (**4**) | 5.30 | 1.49 | 5% VNbCr (**7**) | 7.98 | 2.05 |
| meso-8% VNb (**5**) | 4.65 | 1.77 | 8% VNbCr (**8**) | 8.18 | 2.39 |
| meso-15% VNb (**6**) | 6.72 | 1.37 | 15% VNbCr (**9**) | 12.76 | 2.77 |

of the organometallic was consistently within 3% of that value estimated from the increase in carbon.

Inspection of Table 3 reveals that the carbon content after treatment with bis(benzene)chromium, and hence the Cr loading level, increases monotonically with increased percentage of V in the samples. This is consistent with the increased oxidizing ability of the materials with a higher V content and demonstrates that the oxidizing ability of the walls can be adjusted by the addition of this dopant to the structure.

Figure 7 shows the electron paramagnetic resonance (EPR) spectra of Nb−TMS1 and the mesoporous VNb oxide composites reduced by bis(benzene)chromium. All samples show a large resonance at $g = 1.98$ originating from the bis(benzene)chromium cation. The broadened nature of the resonances suggests that there may be other spin active species present. Figure 8 shows EPR spectra of the sample which was made from mesoporous niobium oxide and 0.001 equiv of bis(benzene)chromium (a) and sample **5** after treatment with 0.001 or 0.003 equiv of bis(benzene) chromium (b, c). The V(IV) hyperfine splittings in the unreduced starting materials are obscured by the bis(benzene)chromium cation resonance at $g = 1.98$, which increases in intensity with higher loading levels. The clear proton hyperfine splittings ($\alpha_H = 3.43$ G, $g = 1.98$), characteristic of the bis(benzene)chromium cation,[31] were obtained in the sample of mesoporous niobium oxide reduced with 0.001 equiv of bis(benzene)chromium. The disappearance of the V (IV) hyperfine splitting in the reduced vanadium-doped meso-

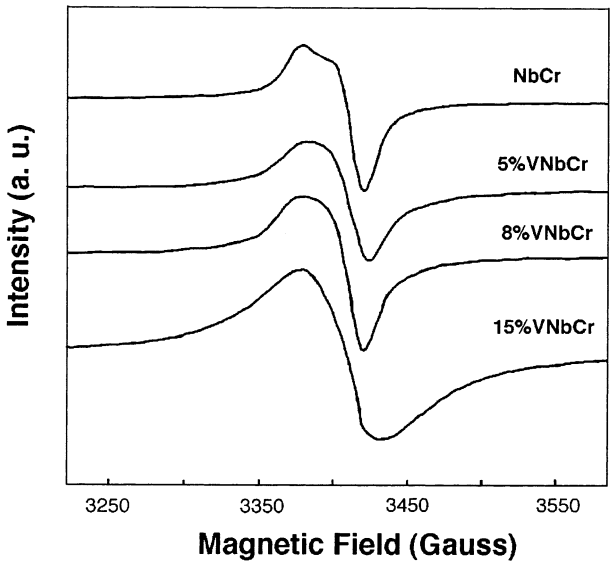


**Figure 7.** EPR spectra of all materials from Figure 6.

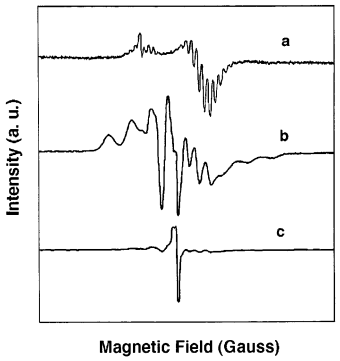


**Figure 8.** Samples of (a) mesoporous niobium oxide treated with 0.001 equiv of bis(benzene)chromium, (b) sample **5** treated with 0.001 equiv of bis(benzene)chromium, and (c) sample **5** treated with 0.003 equiv of bis(benzene)chromium.

porous niobium oxide samples is due to the strong electron−electron interaction in this system because the V(V) in the starting materials had been reduced into V(IV) by bis(benzene)chromium. The peak at $g = 2.00$ from free electrons in the mesostructure, observed in many reduced mesoporous niobium oxides studied in our group, was not resolved in this case, most likely because it is obscured by the strong signal for the bis(benzene)chromium cation. These data indicate that the mesoporous structure was reduced by bis(benzene)chromium to give a new material with V(IV) in the walls and the bis(benzene)chromium cation in the pore channels.

XPS studies of the mesoporous V−Nb oxides after reaction with bis(benzene)chromium (**7**−**9**) provide further evidence of the reduction of the mesostructure. Figure 9a shows the V 2p (1/2, 3/2) region, exhibiting asymmetric emissions centered at 515.0 and 522.0 eV. These emissions are broader and centered at much lower binding energy than those for the unreduced material at ca. 516 eV shown in Figure 4a, indicating a greater degree of reduction to V(IV) by the organometallic in the former materials. The broadness of the emissions suggests that there is still V(V) remaining in the reduced materials and that there are V sites in the

(31) Prins, R.; Reinders, F. J. *Chem. Phys. Lett.* **1969**, *3*, 45.

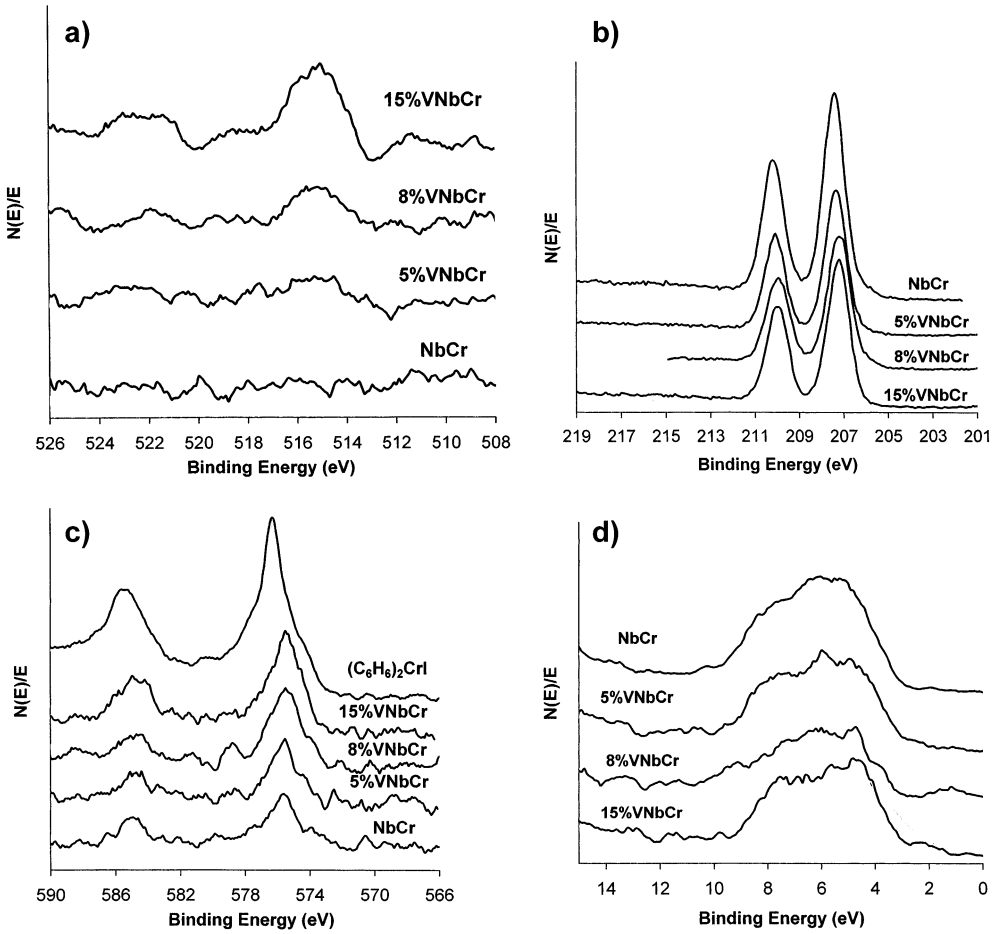


**Figure 9.** XPS spectra of all materials from Figure 6 after treatment with excess bis(benzene)chromium showing the (a) V 2p 1/2 and 3/2 regions, (b) Nb 3d 3/2 and 5/2 regions, (c) Cr 2p 1/2 and 3/2 regions with bis(benzene)chromium iodide for reference, and (d) region near Fermi level.

**Table 4.** Effects of Vanadium Contents on the Conductivity of Bis(benzene)chromium-Reduced Mesoporous V−Nb Oxide Composites

| samples | 0.7 wt equiv[a] ($\Omega^{-1}$ cm$^{-1}$) | 0.1 wt equiv[a] ($\Omega^{-1}$ cm$^{-1}$) | 0.05 wt equiv[a] ($\Omega^{-1}$ cm$^{-1}$) | 0.01 wt equiv[a] ($\Omega^{-1}$ cm$^{-1}$) |
|---|---|---|---|---|
| Nb−TMS1+ $(C_6H_6)_2Cr$ | $1.36 \times 10^{-5}$ | $6.88 \times 10^{-6}$ | $2.26 \times 10^{-6}$ | $4.24 \times 10^{-7}$ |
| **4** + $(C_6H_6)_2Cr$ | $4.52 \times 10^{-6}$ | $1.70 \times 10^{-6}$ | $2.20 \times 10^{-7}$ | insulating[b] |
| **5** + $(C_6H_6)_2Cr$ | $1.13 \times 10^{-6}$ | $5.24 \times 10^{-7}$ | insulating[b] | insulating[b] |
| **6** + $(C_6H_6)_2Cr$ | insulating[b] | insulating[b] | insulating[b] | insulating[b] |

[a] The numbers are the weight ratio of $(C_6H_6)_2Cr$ added to the mesoporous transition metals oxides added to the mesoporous transition metal oxides with 0.7 equiv representing an excess. [b] Insulating indicates the conductivity is lower than $10^{-8}$ $\Omega^{-1}$ cm$^{-1}$.

walls that are perhaps too isolated for reduction by a reagent introduced on the surface of the pore channels. As expected, the intensity of the emissions increases with increased percentage of V. Figure 9b shows the Nb 3d (5/2, 3/2) region. The emissions appear at lower binding energy (207.1 and 209.9 eV) as compared to the starting materials at 207.6 and 210.4 eV. These data indicate that some surface Nb sites have also been reduced by the organometallic. Figure 9c shows the Cr 2p (3/2, 1/2) region of the reduced materials, with emissions at 575.5 and 585.1 eV, consistent with neutral bis(benzene)chromium.[32] The spectrum for bis(benzene)-chromium iodide is shown for comparison. The emission for the bis(benzene)chromium(I) cation in the composites was weak and not clearly resolved, indicating the Cr(0)/Cr(I) ratio is in favor of the neutral species. As predicted from the elemental analysis in Table 3, these emissions increase in intensity as the vanadium component increases in the materials. There is also a small emission at lower binding energy which may be due to Cr metal from minor decomposition pathways. Figure 9d shows the region near the Fermi level with a rough distance to the Fermi level of 3.0 eV for the metal−oxygen sp valence emission.

Table 4 shows the effects of vanadium content in the materials on the room-temperature four point dc conductivity of bis(benzene)chromium-reduced mesoporous V−Nb oxide composites. For each mesoporous oxide composition, samples with 0.01, 0.05, 0.1, and 0.7 (excess) weight equiv of bis-(benzene)chromium were prepared to gauge the effect on conductivity of increasing the Cr while holding the V level constant. Variable-temperature conductivity studies on these materials showed that the conductivity dropped sharply with the decrease of the temperature, indicating that these materials are semiconductors. Materials **1**−**6** were insulating before reduction by the organometallic. Previous work in our group

(32) Binder, H.; Elschenbroich, C. *Angew. Chem. Int. Ed. Engl.* **1973**, *12*, 659.

showed that increasing the loading level of bis(benzene)-chromium in mesoporous niobium oxide from Cr:Nb ratios of 0.01:1 to 0.07:1 led to an increase of conductivity and that the electron transport mechanism appeared to involve a mixed oxidation state bis(benzene)chromium−bis(benzene)-chromocenium phase in the pore channels.[21] Estimations of the bandwidths and Hubbard potentials of these materials do not preclude such a mechanism where the electron moves by a hopping process between the Cr(0) and Cr(I) centers. The insulating nature of mesoporous niobium oxide reduced with varying amounts of alkali metal or cobaltocene suggests that the walls do not participate in the electron transport mechanism. Close inspection of Table 4 shows that materials at a given V loading level show an increase in conductivity with increased bis(benzene)chromium, similar to other reduced mesoporous niobium oxides with alkali metal fulleride[17] or organometallic[18−23] in the pores, which display an increase in conductivity with increased dopant level. While XPS cannot resolve the Cr species in the samples with 0.1, 0.05, and 0.01 equiv of bis(benzene)chromium, solid-state NMR studies presented later in this paper indicate that these materials have an excess of the Cr(I) over Cr(0), contrasting to the materials with 0.7 equiv of organometallic which all have an excess of Cr(0). This, in conjunction with the results in Table 4, strongly suggests that an excess of Cr(0) favors higher conductivity. Materials with alkali metal fullerides in the pores also show a strong dependence of conductivity on the mean oxidation state of the fulleride in addition to the absolute $C_{60}$ loading level. Molecular conductors in general show a strong relationship between conductivity and the electron population the conduction band and, hence, the mean oxidation state of the charge carrying species. Thus, composites with a high Cr(0) to Cr(I) ratio are likely to be more conducting than those with a low Cr(0) to Cr(I) ratio, because of the higher number of Cr 3d conduction electrons in the former system. Paradoxically, Table 4 also reveals a decrease in conductivity with increasing V at a given bis(benzene)chromium loading level. This was unexpected as the samples with more V have a higher absolute Cr content as well as a high Cr(0)/Cr(I) ratio. This trend could be related to a different conductivity mechanism in these materials as compared to the V-free starting materials, in which the V in the walls acts as an electron trap, hindering electron transport through the system.

Figure 10a shows the superconducting quantum interference device (SQUID) magnetometer plots of the magnetic susceptibility versus temperature for the composites **7**−**9**. The hysteresis and slight transition at 10 K in the ZFC branch of the plots indicates some degree of spin glass behavior. Figure 10b shows the variation of inverse magnetic susceptibility with temperature over the temperature range from 6 to 100 K, indicating that these materials obeys the Curie−Weiss law, $\chi_m = C/(T - \Theta)$, where $C$ is the Curie constant and $\Theta$ is the Weiss constant. The effective magnetic moment $\mu_{eff}$ can calculated from the equation $C = N\mu_B^2\mu_{eff}^2/3\kappa$, where $N$ is the Avogadro number, $\mu_B$ is the Bohr magneton, and $\kappa$ is the Boltzman constant.[33] The results are summarized in Table 5. The sample with the highest V and Cr loading (**9**) has the highest number of unpaired electrons of these samples, while the sample made from V-free Nb−TMS1 and bis(benzene)chromium has the lowest number of unpaired electrons and the lowest Cr loading level. This result is also fully consistent with the data from XPS studies. The negative Weiss constant is consistent with spin glass behavior, also observed in other bis(benzene) and bis(cyclopentadienyl) transition metal doped materials studied in our group.[22,23]

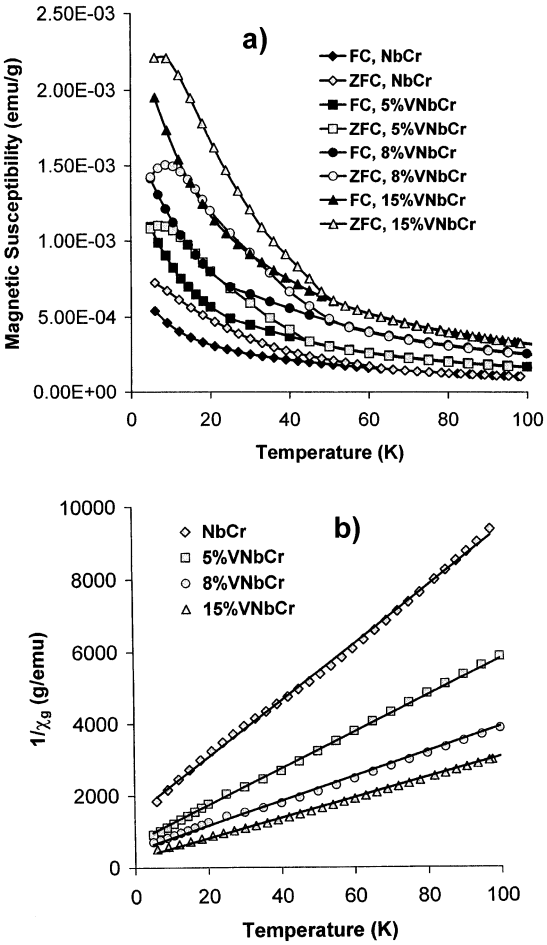


**Figure 10.** SQUID magnetometer plots of (a) magnetic susceptibility versus temperature and (b) variation of inverse magnetic susceptibility with temperature for all materials from Figure 6.

**Table 5.** Curie Constants, Weiss Constants, and Effective Magnetic Moments of the Samples Made from Mesoporous Transition Metal Oxide and Excess Bis(benzene)chromium

| samples | $C$ (emu g$^{-1}$ K) | $\Theta$ (K) | $\mu_{eff}$ |
|---|---|---|---|
| NbCr | 0.0127 | −18.869 | 0.1008 |
| 5% VNbCr (**7**) | 0.0197 | −14.089 | 0.1255 |
| 8% VNbCr (**8**) | 0.0291 | −13.71 | 0.1525 |
| 15% VNbCr (**9**) | 0.0354 | −8.6086 | 0.1682 |

**Solid-State $^2$H NMR Studies on Encapsulate Bis(benzene)chromium Species. (a) Background.** To gain more insight into the nature of the Cr species at loading levels lower than the XPS detection limit and investigate the dynamic behavior of the charge carrying species in the pores,

(33) Chen, C.-W. *Magnetism and Metallurgy of Soft Magnetic Materials*; Dover Publications: New York, 1986.

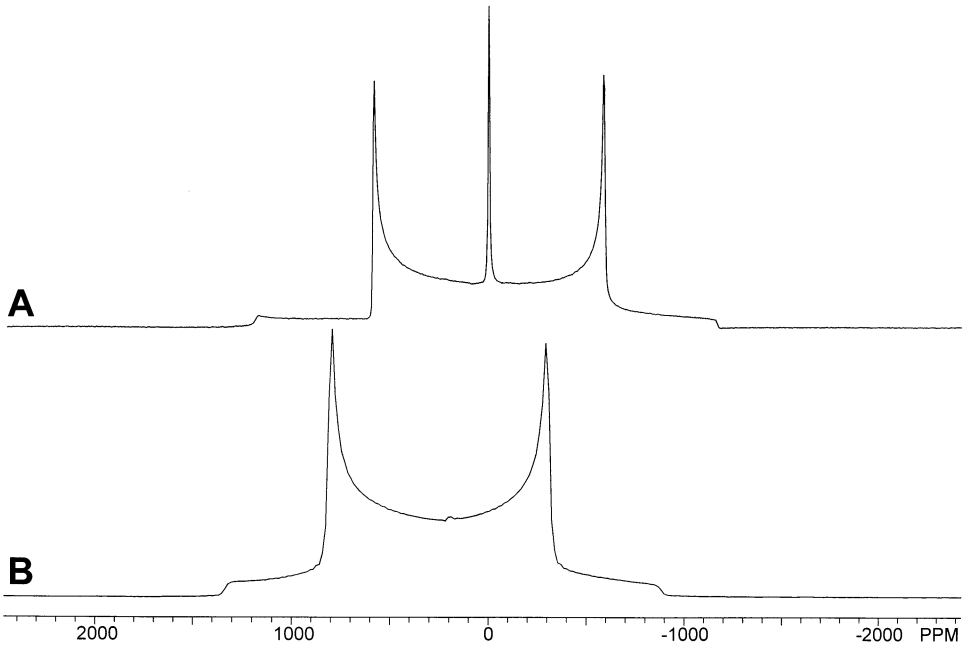


**Figure 11.** Static $^2$H NMR spectra of (A) bis(benzene)chromium(0) and (B) bis(benzene)chromium(I) cations acquired at 9.4 T.

solid-state $^2$H NMR studies were conducted upon pure samples of bis(benzene)chromium(0) and bis(benzene)chromium(I) iodide, as well as mesoporous metal oxides loaded with 0.1 and 0.7 equiv of bis(benzene)chromium(0). Solid-state $^2$H NMR has been applied in many instances to study organic, inorganic, organometallic, biological, and composite materials.[34] Deuterium is a quadrupolar nucleus with a nuclear spin of 1 and has a very small nuclear quadrupole moment ($Q = 2.86 \times 10^{-31}$ m$^2$).[35] Solid-state NMR experiments on this integer spin typically yield Pake-like powder patterns and are influenced by the first-order quadrupolar interaction.

The quadrupolar interaction is a measure of the interaction of the nuclear electric quadrupole moment and surrounding electric field gradients. The electric field gradient (EFG) at a quadrupolar nucleus can be described by a traceless symmetric second-rank tensor, **V**, which has three principal components which are defined such that $|V_{11}| \leq |V_{22}| \leq |V_{33}|$. Since the EFG tensor is traceless, the quadrupolar interaction can be described by two parameters: the quadrupolar coupling constant, $C_Q$, and the quadrupolar asymmetry parameter, $\eta_Q$. The former describes the magnitude of the quadrupolar interaction and is defined as $C_Q = eQeq/h = eQV_{33}/h$, where $eQ$ is the nuclear electric quadrupole moment. The latter describes the axial symmetry of the EFG tensor and is defined as $\eta_Q = (V_{11} - V_{22})/V_{33}$, where $0 \leq \eta_Q \leq 1$.

The quadrupolar interaction at the deuterium nucleus is dependent upon the degree of electronic symmetry. Generally, a nucleus in a spherical site will have a negligible value of $C_Q$, while a site in an increasingly asymmetric electronic environment may have a large value of $C_Q$ and a nonzero value of $\eta_Q$ (indicating a decrease in axial symmetry). The $+1 \leftrightarrow 0$ and $0 \leftrightarrow -1$ NMR transitions are observed in solid-state $^2$H NMR spectra which have overlapping anisotropic first-order patterns and usually span a range on the order of hundreds of kHz, depending upon the magnitude of the quadrupolar interaction. The $^2$H NMR powder patterns can be easily measured with modern pulsed NMR experiments, due to the relatively small quadrupolar interactions. The great benefit of solid-state $^2$H NMR is that dynamic motion of deuterium atoms (and therefore the EFG tensors at the deuterium nuclei) can have a dramatic effect on the appearance of the static $^2$H NMR spectrum. Dynamic simulations can be carried out to extract information on the quadrupolar interaction, molecular motion, and activation energies for a variety of rotational, translational, and diffusion processes.[28,34]

**(b) Characterization of Organometallic Samples.** Solid-state static $^2$H NMR spectra of pure bis(benzene)chromium(0) and the bis(benzene)chromium(I) cation acquired at room temperature are shown in Figure 11. Powder patterns corresponding to two distinct deuterium species are visible in Figure 11A: a large Pake doublet centered at 5.77 ppm; a sharp resonance centered at 7.27 ppm. The former corresponds to $^2$H atoms on a rapidly rotating $\eta^6$-benzene rings in the bis(benzene)chromium(0) complex, and the latter, to free benzene molecules (this peak is set to 7.27 ppm and is useful as an internal $^2$H chemical shift reference). The presence of free benzene molecules likely results from decomposition of the bis(benzene)chromium(0) species. Similar $^2$H NMR spectra identifying residual benzene have previously been observed for the analogous Mo($\eta$-$C_6D_6$)$_2$ complex.[36] In Figure 11B, only a single $^2$H Pake pattern is observed, which corresponds to the $^2$H atoms of the bis(benzene)chromium(I) cation. The chemical shift of this pattern is measured to be 288 ppm. No benzene peak is observed, likely due to the fact that bis(benzene)chromium-

(34) Duer, M. J. In *Annual Reports on NMR Spectroscopy*; Annual Reviews: Palo Alto, CA, 2001; Vol. 43, pp 1−58.
(35) Pyykko, P. *Mol. Phys.* **2001**, *99*, 1617−1629.
(36) O'Hare, D.; Heyes, S. J.; Barlow, S.; Mason, S. *J. Chem. Soc., Dalton Trans.* **1996**, 2989−2993.

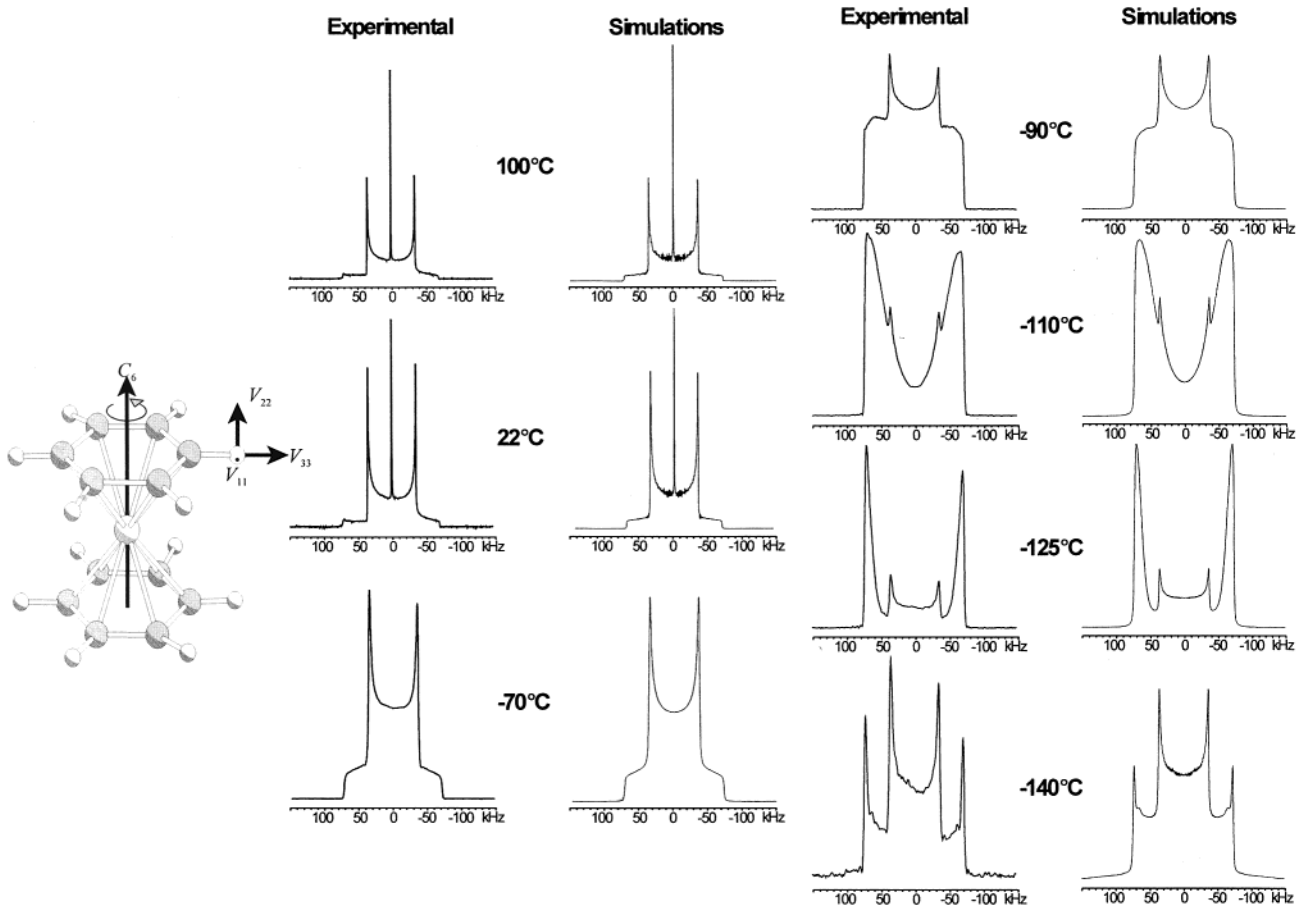


**Figure 12.** Variable-temperature static $^2$H NMR spectra and dynamic simulations of bis(benzene)chromium(0) acquired at 9.4 T.

(I) is an air-stable compound and does not undergo decomposition as readily as bis(benzene)chromium(0). The isotropic chemical shift difference between the Cr(0) and Cr(I) complexes is attributed to the fact that the latter compound is paramagnetic and some unpaired electron spin density is delocalized over the coordinated $\eta^6$ benzene rings, resulting in large high-frequency chemical shifts.[37,38] Similar chemical shift differences were measured by $^1$H MAS NMR experiments conducted upon nondeuterated and partially deuterated samples (not shown). Simple analytical simulations of the $^2$H Pake doublets of bis(benzene)chromium(0) and bis(benzene)chromium(I) yield values of $C_Q = 96$ kHz and $\eta_Q = 0$ and $C_Q = 90$ kHz and $\eta_Q = 0$, respectively. The values of $C_Q$ obtained from analytical simulations are effective quadrupolar coupling constants,[39] which result from the averaging of quadrupolar interaction by dynamic motions, i.e., the rotation of the coordinated benzene ring about the $C_6$ axis. It should be noted that the effective $C_Q$ values of aromatic deuterons are very similar in many bis(benzene) and metallocene complexes. For example, Overweg et al. studied the molecular motion of deuterated ferrocene and cobalt half-sandwich complexes in zeolites and found that values of $C_Q(^2H)$ are around 97 kHz.[40]

Variable-temperature static $^2$H NMR can be used to probe the rotational dynamics and temperature dependence of chemical shift of the various species identified in the room-temperature spectra. Static $^2$H NMR spectra for a sample of pure bis(benzene)chromium(0) with residual benzene-$d_6$ are shown in Figure 12. At room temperature and higher, the Pake doublet for the bis(benzene)chromium(0) and a sharp resonance for isotropically reorienting benzene-$d_6$ are observed (isotropic reorientation averages the $C_Q$ to zero, just like in the liquid phase). As the temperature is decreased to −70 °C, the sharp benzene resonance seems to disappear; however, what is actually occurring is that the benzene is no longer isotropically reorienting but, rather, behaving like a rigid rotor making rapid rotational jumps about the $C_6$ axis. This phenomenon is well documented for benzene loaded into microporous and mesoporous solids.[41,42] As the temperature is further decreased below −70 °C, the benzene $^2$H powder pattern undergoes further dramatic changes, while the bis(benzene)chromium(0) powder pattern changes at a much slower rate.

A good estimate of the unaveraged "real" $C_Q$ of bis(benzene)chromium(0) used in the dynamic simulations is

(37) Blumel, J.; Herker, M.; Hiller, W.; Kohler, F. H. *Organometallics* **1996**, *15*, 3474−3476.
(38) Heise, H.; Kohler, F. H.; Xie, X. L. *J. Magn. Reson.* **2001**, *150*, 198−206.
(39) Penner, G. H.; Chang, Y. C. P.; Grandin, H. M. *Can. J. Chem.* **1999**, *77*, 1813−1820.
(40) Overweg, A. R.; Koller, H.; de Haan, J. W.; van de Ven, L. J. M.; van der Kraan, A. M.; van Santen, R. A. *J. Phys. Chem. B* **1999**, *103*, 4298−4308.
(41) Gedat, E.; Schreiber, A.; Albrecht, J.; Emmler, T.; Shenderovich, I.; Findenegg, G. H.; Limbach, H. H.; Buntkowsky, G. *J. Phys. Chem. B* **2002**, *106*, 1977−1984.
(42) Xiong, J. C.; Maciel, G. E. *J. Phys. Chem. B* **1999**, *103*, 5543−5549.

approximately double the effective $C_Q$ obtained from the analytical simulations,[41,43] whereas unaveraged $C_Q$ of benzene-$d_6$ molecule has been determined from low-temperature $^2$H NMR studies on solid benzene.[44−46] With $C_Q = 191-195$ kHz and $\eta_Q = 0$ for bis(benzene)chromium(0) and $C_Q = 185-195$ kHz and $\eta_Q = 0$ for benzene-$d_6$, the MXQET program was applied to simulate all of the dynamic effects of rotational jumps about a $C_6$ axis on the first-order $^2$H quadrupolar powder patterns and to extract the relevant rate constants describing the reorientation of the rings. To perform such simulations, the orientation of the $^2$H EFG tensor with respect to the molecular frame must be known and the exchange matrix and angles describing the reorientation of the $^2$H EFG tensors must be described. It is well known for many aromatic $^2$H species that the largest component of the EFG tensor, $V_{33}$, points directly along the aromatic C−D bond, with the remaining components, $V_{22}$ and $V_{11}$, directed perpendicular and parallel to the plane of the aromatic ring, respectively.[36,42] In the case of an axially symmetric EFG tensor (i.e., $\eta_Q \approx 0$), the relative orientation of $V_{11}$ and $V_{22}$ is not crucial, and the only factors determining the appearance of the static $^2$H powder pattern are the magnitude of $V_{33}$, the rate at which $V_{33}$ reorients, and the Euler angles determining the relative orientation of $V_{33}$ at different sites. In the case of rotational jumps about the $C_6$ axis of benzene or benzene coordinated to chromium, the Euler angles can be set as $\varphi = 0$, 60, 120, 180, 240, or 300°, $\theta = 90°$, and $\rho = 90°$. The final result of applying these Euler angles is shown schematically in Figure 12, where the variable angle $\varphi$ ensures that six different sites about an ideal hexagon are sampled, while $\theta$ tips $V_{33}$ into the plane of the ring and $\rho$ orients $V_{22}$ perpendicular to the ring plane. An Arrhenius plot, i.e., for $k = A \exp(-E_a/RT)$, of ln $k$ vs $1/T$, yields an activation energy for rotation of $E_a = 10.0$ kJ mol$^{-1}$ and an activation parameter $A = 2.3 \times 10^{10}$ s$^{-1}$ for bis(benzene)chromium(0) and $E_a = 30.5$ kJ mol$^{-1}$ and $A = 4.0 \times 10^{15}$ s$^{-1}$ for "free" benzene-$d_6$ trapped in the solid bis(benzene)chromium(0). The values for bis(benzene)chromium(0) are in reasonably good agreement with previously measured results of $E_a = 19.6$ kJ mol$^{-1}$ for ($\eta^6$-$C_6D_6$)Cr(CO)$_3$,[45] 15.5 kJ mol$^{-1}$ for bis(benzene)chromium(I) iodide,[47] and 18.8 kJ mol$^{-1}$ in bis(benzene)chromium(0).[48] The $E_a$ of the "free" benzene-$d_6$ molecule is higher than what was found in Buntkowsky et al. (16.8 kJ mol$^{-1}$)[41] and Vold et al. (16.5 kJ mol$^{-1}$),[44] though our measurements were made upon residual benzene resulting from decomposition of bis(benzene)chromium(0) and their measurements were made upon pure solid benzene-$d_6$ over a larger temperature range.

(43) O'Brien, S.; Tudor, J.; O'Hare, D. *J. Mater. Chem.* **1999**, *9*, 1819−1824.
(44) Ok, J. H.; Vold, R. R.; Vold, R. L.; Etter, M. C. *J. Phys. Chem.* **1989**, *93*, 7618−7624.
(45) Aliev, A. E.; Harris, K. D. M.; Guillaume, F. *J. Phys. Chem.* **1995**, *99*, 1156−1165.
(46) Mantsch, H. H.; Saito, H.; Smith, I. C. P. *Prog. Nucl. Magn. Reson. Spectrosc*. **1977**, *11*, 211−271.
(47) Howard, J.; Robson, K.; Waddington, T. C. *J. Chem. Soc., Dalton Trans.* **1982**, 977−984.
(48) Campbell, A. J.; Fyfe, C. A.; Haroldsmith, D.; Jeffrey, K. R. *Mol. Cryst. Liq. Cryst.* **1976**, *36*, 1−23.

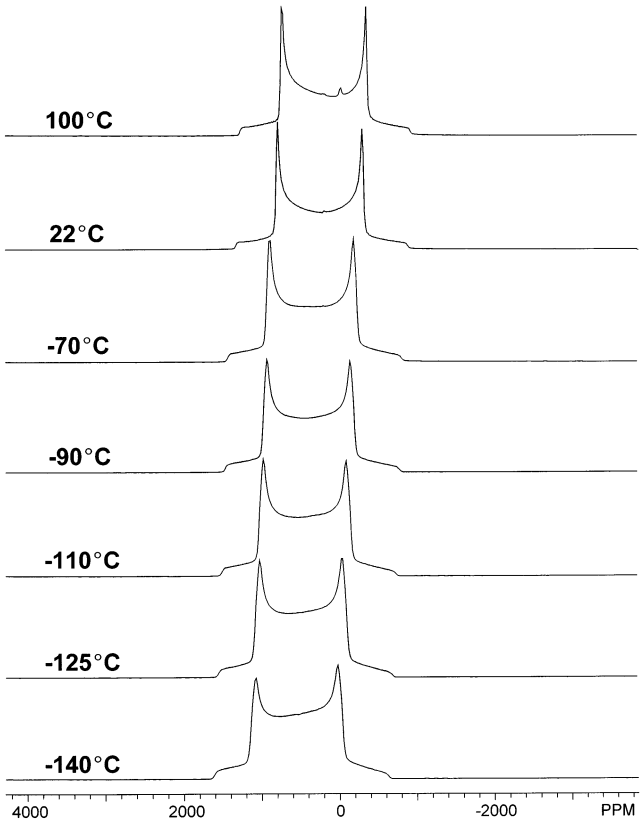


**Figure 13.** Variable-temperature static $^2$H NMR spectra of bis(benzene)-chromium(I) iodide acquired at 9.4 T.

Variable-temperature static $^2$H powder patterns for bis(benzene)chromium(I) (Figure 13) change less dramatically than those for bis(benzene)chromium(0), since there is much less residual benzene due to the relatively higher stability of the bis(benzene)chromium(I) cation. Only in the spectrum acquired at +100 °C is a small benzene-$d_6$ resonance detected at ca. 7.3 ppm. Since the bis(benzene)chromium(I) cation is paramagnetic, there is a large temperature-dependent chemical shift: the $^2$H resonance shifts to higher frequency as the temperature is lowered. The Pake doublet of bis(benzene)chromium(I) shifts from 243 ppm at +100 °C to 590 ppm at −140 °C. Graphing $\delta_{iso}$ as a function of $1/T$ yields a linear plot consistent with Curie−Weiss $1/T$ chemical shift dependence for paramagnetic ions (Figure 14).

**(c) Characterization of Composite Samples.** Figure 15 shows the experimental variable-temperature $^2$H NMR spectra of a mesoporous metal oxide loaded with 0.1 equiv of bis(benzene)chromium(0), along with the corresponding analytical simulations. At room temperature, there appear to be two distinct powder patterns: a Pake doublet and a narrow powder pattern. The narrow pattern corresponds to the isotropically reorienting benzene-$d_6$ molecules at ca. 7.3 ppm. The intensity of this sharp benzene powder pattern decreases at lower temperatures, and any contribution to the overall powder pattern intensity seems to disappear at −90 °C and lower. The absence of broad powder patterns for benzene-$d_6$ at lower temperatures likely indicates its low abundance in the loaded sample and suggests that much of the bis(benzene)chromium(0) is rapidly converted to bis(benzene)chromium(I) upon loading. The Pake doublet

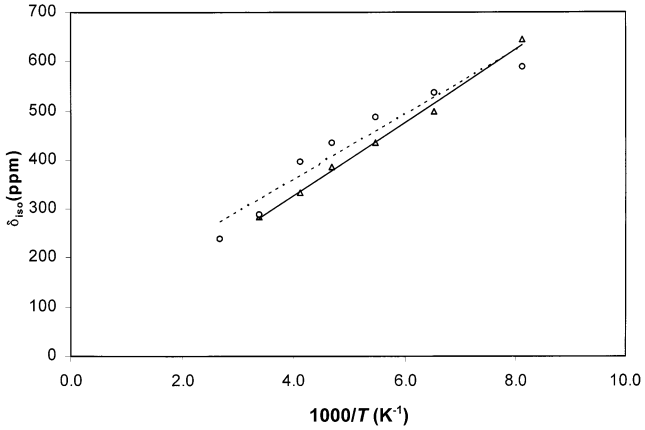


**Figure 14.** Temperature dependence of the paramagnetic $^2$H NMR chemical shift of bis(benzene)chromium(I) iodide (○) and mesoporous metal oxides loaded with 0.1 equiv of bis(benzene)chromium(0) (△).

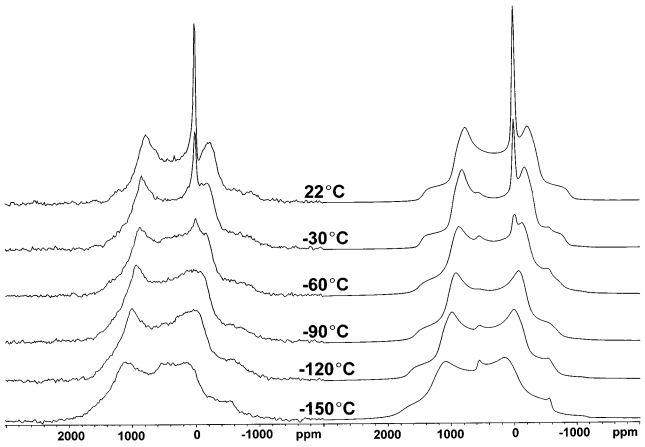


**Figure 15.** Variable-temperature static $^2$H NMR spectra (left) and simulations (right) of mesoporous metal oxides loaded with 0.1 equiv of bis(benzene)chromium(0) acquired at 9.4 T.

corresponds to the bis(benzene)chromium(I) cation, and it shifts in the high-frequency direction with decreasing temperature, from 285 ppm at room temperature to 645 ppm at −150 °C ($C_Q$ varies from 92 to 95 kHz, and $\eta_Q$ varies from 0.1 to 0.15). This shift of the Pake doublet as the temperature decreases confirms the presence of bis(benzene)chromium(I) cation. At −30 °C and lower, the presence of a new powder pattern is detected, centered at approximately 5 ppm and with the shape of a Pake doublet that can be simulated with $C_Q = 94$ kHz and $\eta_Q = 0.01$. This powder pattern can be assigned to the bis(benzene)chromium(0) species which has not been oxidized to bis(benzene)chromium(I), since the powder pattern has NMR parameters identical to those of pure bis(benzene)chromium(0) and does not display the low-temperature powder patterns associated with benzene-$d_6$. The $^2$H powder pattern of bis(benzene)chromium(0) is not apparent in the room-temperature spectrum due to overlap of the Pake doublets of the Cr(0) and Cr(I) species and the fact that the ratio of bis(benzene)chromium(0) to bis(benzene)chromium(I) is about 1:10. $^2$H MAS NMR experiments on this sample were relatively unsuccessful at resolving the individual species, though it is clear from the simulations of the static spectra shown in Figure 15 that the bis(benzene)chromium(0) species is present in low abundance. A variable-temperature plot of $\delta_{iso}$ of the loaded bis(benzene)chromium(I) cation as a function of $1/T$ shows the same temperature dependence as for the pure bis(benzene)chromium(I) cation (Figure 14).

For a higher loading level of bis(benzene)chromium(0) (0.7 equiv), $^2$H NMR experiments reveal that the amount of bis(benzene)chromium(0) present in the metal oxide is much higher than the bis(benzene)chromium(I) cation, in contrast to the low loading sample. However, there is still evidence of the bis(benzene)chromium(I) cation resulting from oxidation of bis(benzene)chromium(0) (Figure 16). Three different $^2$H species are resolved. The narrow resonance is assigned to benzene-$d_6$ with a chemical shift of ca. 7.3 ppm. The intense Pake doublet centered at ca. 6 ppm ($C_Q = 96-97$ kHz and $\eta_Q = 0$) corresponds to the bis(benzene)chromium(0) species, and the smaller Pake doublet exhibiting the same temperature-dependent chemical shifts as the aforementioned examples has chemical shifts ranging from 240 to 591 ppm from +100 to −140 °C ($C_Q = 90-91$ kHz and $\eta_Q = 0-0.06$) and corresponds to the bis(benzene)chromium(I) cations. The narrow resonance again seems to disappear at lower temperatures, though benzene-$d_6$ is considerably more abundant than in the low loading species (notably apparent in the low-temperature spectra). Around −70 °C and lower, evidence of a small amount of the bis(benzene)chromium(I) cations can be detected shifting over a 350 ppm range from 100 to −140 °C. Though not strictly quantitative, the deconvolution of the low-temperature simulations reveal that the ratio of benzene-$d_6$:bis(benzene)chromium(0):bis(benzene)chromium(I) can be roughly estimated to be about 8:30:1.

This set of experiments indicates that loading with low and high levels of bis(benzene)chromium(0) into the mesoporous metal oxides produces a mixed-oxidation state composite material. In both cases, bis(benzene)chromium(I) cations are produced and both Cr(0) and Cr(I) species coexist. Low loading levels result in almost complete conversion of bis(benzene)chromium(0) to bis(benzene)chromium(I), whereas high loading levels contain a fair amount of unreacted bis(benzene)chromium(0) and residual benzene-$d_6$, possibly arising from the small amount of decomposition of the organometallic to Cr metal detected in the XPS. The constancy of the $^2$H Pake doublet patterns indicates that the bis(benzene)chromium species are not isotropically reorienting in this composite material; rather, the coordinated benzene rings undergo rapid reorientation about the $C_6$ axes and the molecules are fixed in position in a manner comparable to the pure compounds. The lack of translational mobility and isotropic tumbling in the Cr species on the NMR time scale suggests that for outer-sphere electron transfer to occur the organometallic charge carriers must be in close proximity to one another or that the walls may be involved in mediating local electron-hopping processes. Many mixed oxidation state semiconductors, such as $Eu_2S_3$,[49] show a time averaging of the species present which is consistent with electron transfer occurring rapidly between the sites. The involvement of the walls in electron hopping

(49) Cox, P. A. *The Electronic Structure and Chemistry of Solids*; Oxford Science Publications: Oxford, Great Britain, 1987.

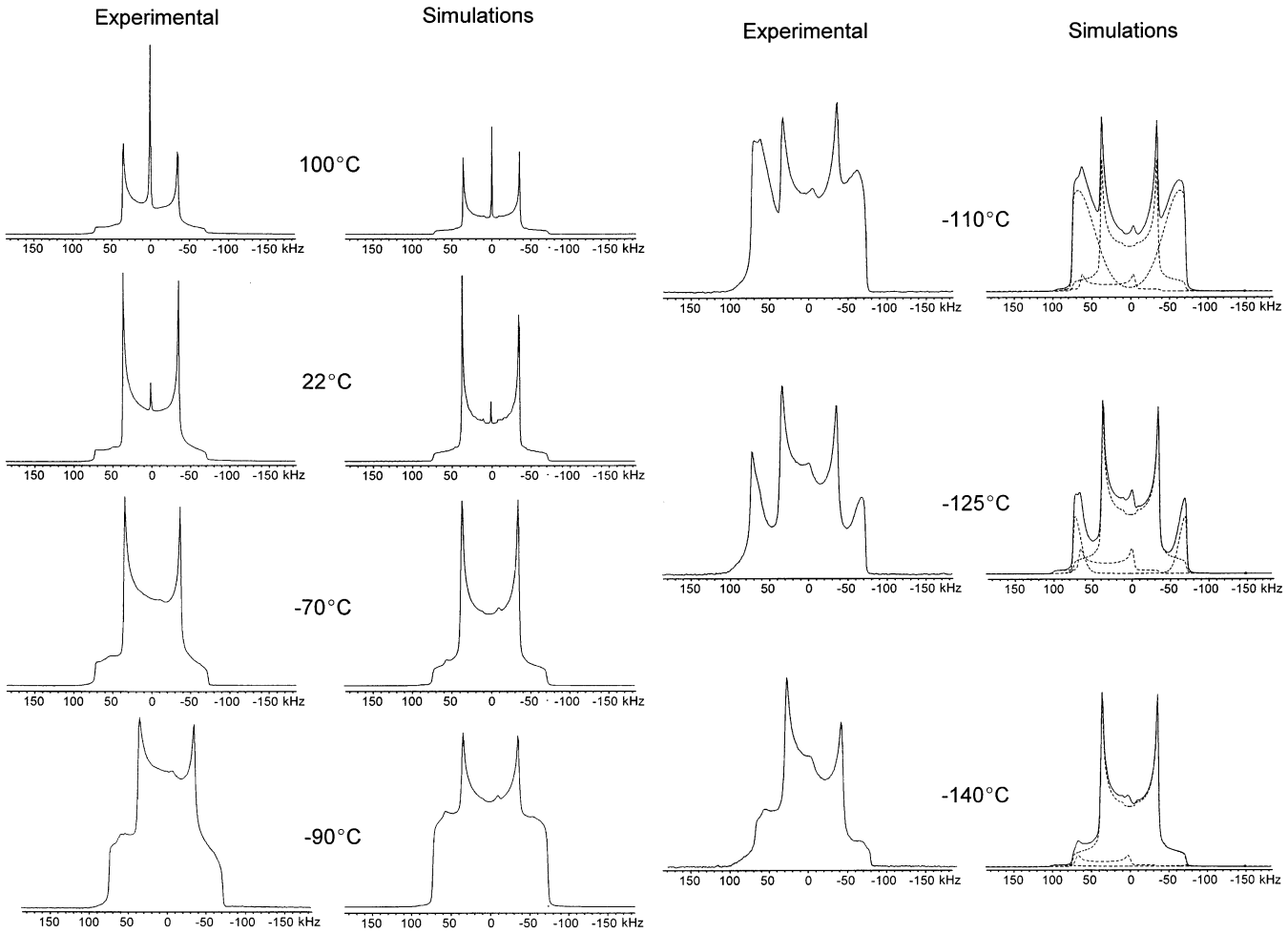


**Figure 16.** Variable-temperature static $^2$H NMR spectra and simulations of mesoporous niobium oxides loaded with 0.7 equiv of bis(benzene)chromium(0) acquired at 9.4 T.

is contrary to our previous model in which the reduced walls were considered to be too insulating because of Anderson localization to observe long-range conductivity. However, it may be possible that short-range electron transfer in the walls can occur, mediating local electron hopping through the walls over a long enough range to bridge the physical distance between the Cr centers to allow electron transfer through the network of organometallic species in the pores. This is certainly consistent with the observation that increased levels of V hinder conductivity, as this necessitates involvement of the walls, possibly with V(IV) acting as a spin trap; however, to clarify this hypothesis more studies are necessary.

## Conclusion

In summary, we have synthesized a new series of mesoporous mixed V−Nb oxides and reduced these materials with bis(benzene)chromium. The increased amount of organometallic absorbed with increased V(V) shows that it is possible to tune the oxidizing strength of the walls of mesoporous niobium oxide by varying the amount of V in a new family of mesoporous V−Nb oxides. This property allowed us to study the effect of a composition on the conductivity and magnetic properties of these composites. The conductivity depended more on the ratio between bis(benzene)chromium and the corresponding cation than on absolute loading level, suggesting that the mean oxidation state of the Cr species was the crucial parameter in governing conductivity. High levels of V, however, were found to lead to insulating behavior regardless of the amount and nature of the Cr species present. Solid-state $^2$H NMR studies showed evidence for both Cr species at all loading levels studied and demonstrated that these species were largely static within the pore structure of the material.

**Acknowledgment.** The Petroleum Research Fund, administered by the American Chemical Society, is thanked for funding. The NSERC and the Ontario Premiere's Research Excellence Program are also thanked for financial support. R.W.S. thanks the NSERC for research funding in the form of an Operations Grant and the Canadian Foundation for Innovation, Ontario Innovation Trust, and University of Windsor for funding the solid-state NMR laboratory at the University of Windsor.

IC020559V